AIAA SciTech Forum
11–15 & 19–21 January 2021, VIRTUAL EVENT
AIAA Scitech 2021 Forum

10.2514/6.2021-1590

Development of an Open-source Flutter Prediction Framework for the Common Research Model Wing

Brandon Crow*, Jethro Nagawkar†, and Leifur Leifsson‡
Iowa State University, Ames, Iowa, 50011, USA

Andrew Thelen§
University of Dayton Research Institute, Dayton, Ohio, 45469, USA

Predicting aeroelastic flutter during the early stages of the aircraft design process is important to help avoid costly problems that may appear later in the design process. By using multifidelity modeling, a relatively cheap flutter analysis can be performed by using the doublet lattice method and the time-accurate Euler equations. This strategy has already been shown to alleviate the cost of transonic flutter prediction. This paper describes the work that has been done so far to make an implementation of this prediction framework that is open-source and accessible to a broader community of researchers. The first half of the framework has been implemented and is described in this paper. An overview of the entire framework is given first. This is followed by the methods section which introduces the theory of the framework and how it has been implemented. The open-source implementation is then verified with the AGARD 445.6. The results of the AGARD 445.6 wing are compared against the results of a closed-source implementation as well as data from the literature. The open-source implementation is also used to obtain results on a version of the undeflected Common Research Model (uCRM) wing. The paper concludes by outlining the work that is left and the anticipated challenges that must be overcome.

Nomenclature

$\mathbf{B}$	=	Damping matrix
$\mathbf{M}$	=	Mass matrix
$\mathbf{K}$	=	Stiffness matrix
$\boldsymbol{q}$	=	Displacement in structural degrees of freedom
$\boldsymbol{f}$	=	Aerodynamic loads in structural degrees of freedom
$\boldsymbol{\Phi}$	=	Mode shape matrix
$\bar{\boldsymbol{M}}$	=	Generalized mass matrix, $(\boldsymbol{\Phi}^{\boldsymbol{T}}\boldsymbol{M}\boldsymbol{\Phi})$
$\bar{\boldsymbol{B}}$	=	Generalized damping matrix, $(\boldsymbol{\Phi}^{\boldsymbol{T}}\boldsymbol{B}\boldsymbol{\Phi})$
$\bar{\boldsymbol{K}}$	=	Generalized stiffness matrix, $(\boldsymbol{\Phi}^{\boldsymbol{T}}\boldsymbol{K}\boldsymbol{\Phi})$
$\boldsymbol{\eta}$	=	Generalized displacements in structural modes, $(\boldsymbol{\Phi q})$
$\boldsymbol{F}$	=	Generalized aerodynamic forces in structural modes, $(\boldsymbol{\Phi}^{\boldsymbol{T}}\boldsymbol{f})$
$\mathbf{Q}$	=	AIC matrix in modal coordinates
q	=	Dynamic pressure, $(\frac{1}{2}\rho V^2)$ [kg/(m-s^2)]
k	=	Reduced frequency, $(\omega b/V)$
M	=	Freestream Mach number, [-]
ω	=	Circular frequency, [rad/s]
b	=	Reference length (usually airfoil semi-chord), [m]
V	=	Flow velocity, [m/s]
ρ	=	Freestream density, [kg/m^3]
$b_{\text{semi-span}}$	=	Wing semi-span, [m]

*BS Student, Department of Aerospace Engineering, AIAA Student Member.
†Ph.D. Student, Department of Aerospace Engineering, AIAA Student Member.
‡Associate Professor, Department of Aerospace Engineering, AIAA Senior Member.
§Postdoctoral Researcher, AIAA Member.

I. Introduction

Aerodynamic flutter is an important aspect during the conceptual design of any modern aircraft, especially transonic transport aircraft [1]. When flutter occurs, a diverging aeroelastic response is created where there is a net gain of energy to a structure's modes of vibration. This results in dangerous structural oscillations that need to be accounted for during the design of an aircraft. Aerodynamic nonlinearities caused by shock waves and flow separation significantly affect the speed at which flutter can occur. These effects cause flutter speed to decrease in the transonic flight regime; this phenomenon is referred to as *transonic dip* [2]. Furthermore, the complex nature of the physics involved makes it difficult to simulate and predict when flutter will occur. Being able to predict flutter during the conceptual design phase would save considerable amounts of time and money by helping to ensure that flutter does not become an issue later in the design cycle. However, modeling flutter in the transonic flight regime requires significant computational resources, resulting in a unique challenge to aircraft designers.

The focus of this work is to implement the flutter analysis framework presented by Thelen et al. [3] using open-source analysis codes. The framework makes accurate but fast flutter boundary predictions [3] by using mode-based simulations in conjunction with multifidelity modeling. This framework was originally implemented with NASTRAN [4] and FUN3D [5], but this paper presents results that were obtained from MYSTRAN [6] and SU2 [7], which are both open-source codes*.

This paper outlines the progress that has been made on the first half of the established flutter prediction framework [3]. The methods section gives an overview of the flutter analysis workflow, followed by a description of the structural and aerodynamic modeling that is needed to predict flutter. This is followed by the results section containing the results obtained on the AGARD 445.6 wing which will be used for verification. Results are also presented for a wing that was used by Beran et al. [8] to demonstrate multifidelity approaches for design. The model is based on the high-aspect ratio (13.5) undeflected common research model (uCRM-13.5) published by the University of Michigan MDO Lab [9, 10]. The results obtained for this version of the uCRM-13.5 wing will valuable since the uCRM-13.5 is a contemporary, transonic wing design. The uCRM-13.5 results presented here will also serve as a good reference while finishing the framework implementation. Finally, the paper concludes with a summary of the work done and future work that is planned in order to complete the implementation of the flutter prediction framework.

II. Methods

This section outlines the methods used in this work. First, the entire workflow of the flutter analysis framework is summarized. This is followed by a description of the structural and aerodynamic modeling of the AGARD 445.6 and uCRM-13.5 wings. The last section briefly describes the AIC matrix calculation and how multifidelity modeling can be used with the p-k method to predict flutter.

A. Flutter analysis workflow

An overview of the flutter prediction process that was used by Thelen et al. [3] is shown in Fig. 1. This paper will focus on the work done on the first half of the framework: starting with the design variables and concluding with the structural and aerodynamic analyses. The framework uses mode-based modeling to predict flutter for airfoils and wings. Although many advanced methods for computing aeroelastic behavior use coupled fluid and structural simulations, mode-based modeling can reduce the computational cost of flutter prediction. In a fluid-structure interaction (FSI) analysis, the transient, nonlinear flow solution is progressed in small increments, and periodically the calculated aerodynamic forces are mapped to the structural model, which then yields updated deflections. Mode-based modeling on the other hand allows a single assessment of the structure's modes of vibration before running computational fluid dynamics (CFD) simulations. By simulating harmonic oscillations in each vibrational mode, it is possible to obtain the relationship between the aerodynamic loads and the structural displacement [3]. This step is represented in Fig. 1 by the step titled "Evaluate aerodynamic response of the oscillating structure". This relationship can be expressed in terms of the generalized aerodynamic influence coefficients (AIC). The AIC terms are, in general, functions of reduced frequency, k, and freestream Mach number, M. By simulating harmonic motion for a range of reduced frequencies and Mach numbers, a database of AIC matrices is generated and flutter information can then be found using the p-k method [3].

One of the most expensive parts of this process is generating the AIC database. The AIC matrices are functions of reduced frequency and freestream Mach number but many of these simulations may have similar flow fields. By

*Code, meshes, and simulation files can be found on the Iowa State CODE Lab Github Page: `https://github.com/CODE-Lab-IASTATE/CRM_Flutter_Prediction_Framework`

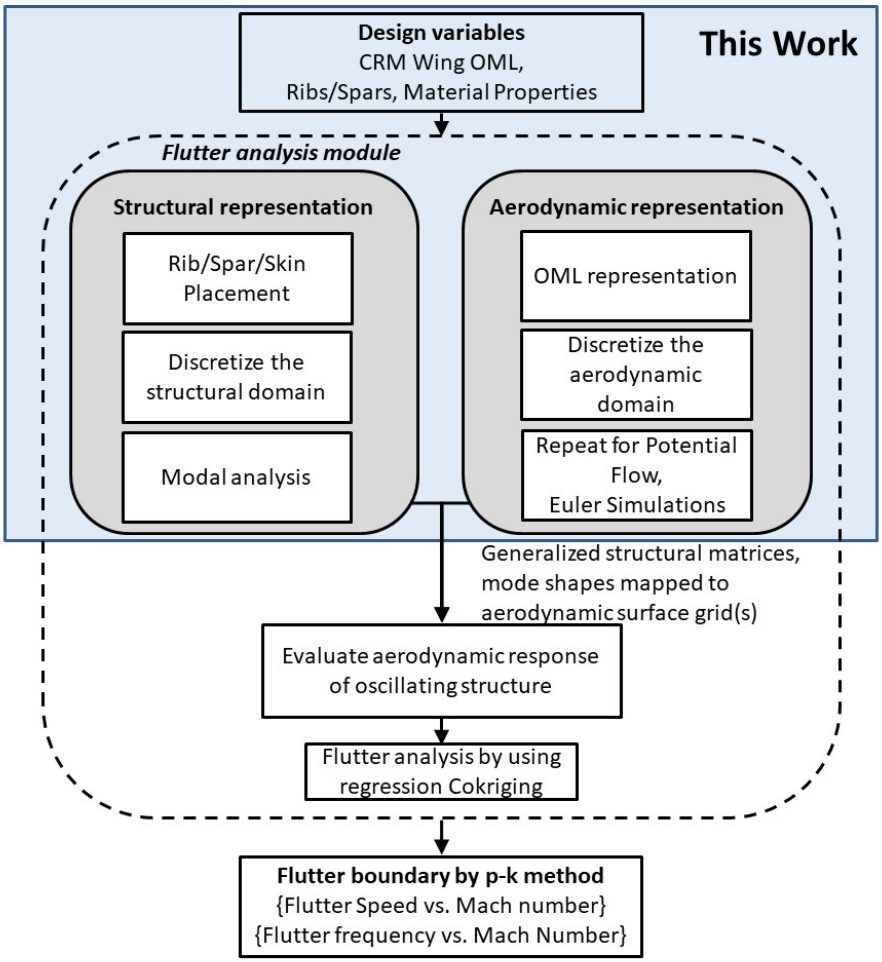

Fig. 1 A flowchart of the flutter analysis workflow

using a multifidelity model, Thelen et al. [3] showed that it is possible to accurately predict the flutter boundary while alleviating the computational cost by using two different aerodynamic models. This was achieved by using many linear models like the doublet lattice method (DLM) [4, 11, 12] and a small number of high fidelity models such as the Euler simulations. Thelen et al. [3] used a cokriging [13] approach with these two different aerodynamic models to represent the AIC matrices.

It was mentioned earlier that this paper will focus on the first half of the framework, concluding with the structural and aerodynamic analysis of each case. Each discipline requires a different representation of a model, and the models for each discipline must be consistent with one another. It must also be possible to change or modify parameters quickly in order to run subsequent analysis on a design. The engineering sketch pad (ESP) [14] is a solid-modeling software that was created to try to address many of these issues and will be used in this work to generate the representations of both the AGARD 445.6 wing and the uCRM-13.5 wing. The computational aircraft prototype synthesis (CAPS) project connects with ESP and is responsible for linking the analysis and meshing disciplines to the ESP geometry model. An instance of a design in ESP therefore contains the representations that are needed for coupled aerostructural analyses. For example, ESP allows a single model for the AGARD 445.6 wing to be generated, consisting of a structural representation and an aerodynamic representation which are geometrically consistent with one another. The python extension module for CAPS (pyCAPS) [15] is used in this work to pass the representations through the respective software packages that are responsible for discretizing the geometry and performing the disciplinary analyses. Furthermore, model connectivity and other metadata is handled internally by CAPS to enable the coupling and data transfer associated with multiple disciplines.

The pyCAPS [15] examples provided with ESP/CAPS were used as a template to perform the aerostructural analysis. One example script used FUN3D and MYSTRAN to perform an aeroelastic modal analysis. The first portion of this example script was used as a template to perform the structural analysis and map the mode shapes to the FUN3D CFD surface grid. CAPS is then used to setup a CFD analysis in SU2 with the same mesh and configuration parameters. At this point, the mode shape information associated with FUN3D is used to finish preparing the SU2 simulations. Currently, an in-house script does this by writing the mesh motion files that are used for running SU2.

B. Structural modeling

The prediction framework begins by the specification of the design variables for the wing of interest. This includes a description of the outer mold line (OML) and the structural representation of the wing. A modal analysis is then performed on the structure which begins with the structural equations of motion for each degree of freedom. These equations are written in the form

$$\mathbf{M}\ddot{\mathbf{q}} + \mathbf{B}\dot{\mathbf{q}} + \mathbf{K}\mathbf{q} = \mathbf{f}, \tag{1}$$

where $\mathbf{M}$, $\mathbf{B}$, and $\mathbf{K}$ are the structure's inertial, damping, and stiffness matrices respectively, and $\mathbf{q}$ and $\mathbf{f}$ are the displacements and aerodynamic loads respectively. Performing a modal analysis yields information on the structure's mode shape matrix, $\mathbf{\Phi}$, and the structural equations of motion can be written in the general form

$$\mathbf{\Phi}^T\mathbf{M}\mathbf{\Phi}\ddot{\boldsymbol{\eta}} + \mathbf{\Phi}^T\mathbf{B}\mathbf{\Phi}\dot{\boldsymbol{\eta}} + \mathbf{\Phi}^T\mathbf{K}\mathbf{\Phi}\boldsymbol{\eta} = \mathbf{\Phi}^T\mathbf{f}, \tag{2}$$

or

$$\bar{\mathbf{M}}\ddot{\boldsymbol{\eta}} + \bar{\mathbf{B}}\dot{\boldsymbol{\eta}} + \bar{\mathbf{K}}\boldsymbol{\eta} = \mathbf{F}, \tag{3}$$

where $\boldsymbol{\eta}$ and $\mathbf{F}$ are the generalized displacements and generalized aerodynamic forces (GAF) in each mode, respectively. These equations will be solved with an eigenvalue-based approach. For small displacements, a linearized stability formulation is also used so that f is a linear function of η. The ratio f/η will be assumed to be proportional to a frequency-dependent complex scalar. The GAF matrix is then replaced by a complex matrix of generalized aerodynamic influence coefficients (GAIC), $\mathbf{Q}$, times the displacement

$$\bar{\mathbf{M}}\ddot{\boldsymbol{\eta}} + \bar{\mathbf{B}}\dot{\boldsymbol{\eta}} + \bar{\mathbf{K}}\boldsymbol{\eta} = q\mathbf{Q}(k)\boldsymbol{\eta}, \tag{4}$$

where q is dynamic pressure and k is reduced frequency. The GAIC terms are functions of mach number and reduced frequency k, so a database of AIC values is generated by running CFD simulations accross the Mach-reduced frequency design space.

In this work, the wing geometry and structural definition will be made in ESP/CAPS. pyCAPS will then be used to setup and perform the structural anslysis. First, the engineering geometry aerospace design system (EGADS) [16] is used to discretize the structural model. The structural meshes for the AGARD 445.6 wing and the uCRM-13.5 wing are shown in Fig. 2. The AGARD 445.6 wing structure is modeled with shell elements located on the outer surface of the wing, while the uCRM-13.5 wing structure is modeled with three structural ribs along the span and 52 ribs from the wing-fuselage junction to the wing tip. MYSTRAN [6] is then used to compute the mode shapes. After the modal analysis is performed, pyCAPS is used to transfer the mode shapes onto the FUN3D surface mesh.

C. Aerodynamic modeling

The linearized stability formulation assumes the relationship between the aerodynamic forces and the displacement to be

$$\boldsymbol{F} = q\boldsymbol{Q}(k)\boldsymbol{\eta}. \tag{5}$$

Knowing $\boldsymbol{\eta}$ and $\boldsymbol{F}$ allow the values in the $\boldsymbol{Q}$ matrix to be found. To account for unsteady aerodynamics like those that are encountered in the transonic regime, CFD-based results will be obtained through forced harmonic motion. Due to the sinusoidal nature of the motion, aerodynamic forces will lag behind the structural deformation so $\boldsymbol{Q}$ will have complex terms. To accurately obtain the terms in the matrix $\boldsymbol{Q}$, two cycles of motion will be simulated for each mode and each cycle will have twenty time steps. These values were chosen as a starting point to demonstrate the process.

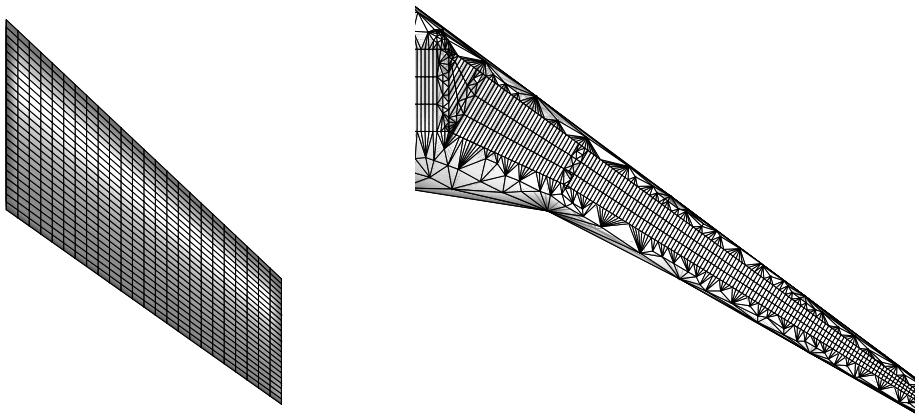

(a) **(b)**

Fig. 2 Structural meshes: (a) AGARD 445.6, and (b) uCRM-13.5

To begin, a steady state solution is found to serve as a starting point for the prescribed motion simulations. Next, each mode shape is mapped to the aerodynamic surface grid. The displacements for each mode are scaled such that the displacement of any point is no more than about 1% of the root chord. Next, the motion files are written for SU2. For each mode, there are two cycles of motion that each contain 20 time steps, so 40 mesh motion files are written per mode. Finally, the user (or an external program) can prescribe values for Mach number, M, and reduced frequency, k. The time step size for the motion is then determined. The motion of each mode is then simulated to obtain the flow field variables. Each mode has 40 flow field solutions corresponding to the 40 time steps. After obtaining the flow fields associated with each mode and time step, the generalized aerodynamic forces in each mode are obtained by integrating the surface pressure over time [3].

The aerodynamic analyses of the AGARD 445.6 and uCRM-13.5 wings were performed through the use of ESP/CAPS and some in-house scripts. The in-house scripts were used to help setup the SU2 simulation files. For each analysis, AFLR4 [17] is used to generate the aerodynamic surface mesh (Fig. 3), while AFLR3 [17] is used to generate the volume mesh. The mode shapes obtained from MYSTRAN [6] are then mapped to the surface grid.

At this point, the in-house script takes over. The first thing the in-house script does is write the mesh motion files for each time step. SU2's mesh motion capabilities were used for the harmonic simulations. Unlike FUN3D, SU2 requires a mesh motion file for each time step. To obtain the mesh motion files for SU2, the values of X, Y, Z, dX, dY, dZ for each node are read from the FUN3D mode shape files. The X, Y, and Z values are the location of each node while the dX, dY, and dZ values are the displacements of each node. To convert these to a form readable by SU2, the final X, Y, and Z locations of the nodes are written. This process is done for each time step and for each mode. A scaling factor is used when writing the mesh motion files so that the maximum displacement of the wing is 1% of the root chord.

The user now specifies the values of Mach number, M, and reduced frequency, k, through the in-house script. The harmonic simulations are now executed. Convergence for each time step is set to a maximum of 110 subiterations or until the density residual is reduced by six orders of magnitude, whichever occurs first. The mesh motion files are independent of Mach number and reduced frequency so when updating values of Mach number and reduced frequency, the SU2 configuration file is all that needs updating.

D. AIC matrix calculation

As outlined above, once the mode shapes are found, harmonic simulations are performed at specific reduced frequencies and Mach numbers. Following the aerodynamic analyses, the next step in the flutter prediction framework would be to quantify the relationship between the aerodynamics and displacement through the time-dependent GAF matrix. The complex GAF terms can be divided by the complex representation of the generalized displacement, $\boldsymbol{\eta}$, to obtain the GAIC matrix terms. The most complex part of this process is computing the generalized aerodynamic forces. Finding these matrix terms involves integrating the pressure forces on the wing as they vary in time. In FUN3D, this was done by using each surface element's surface normal vector. In SU2 however, this information is not publicly exposed to the user. The authors believe that it may still be possible to extract this information by using SU2's python

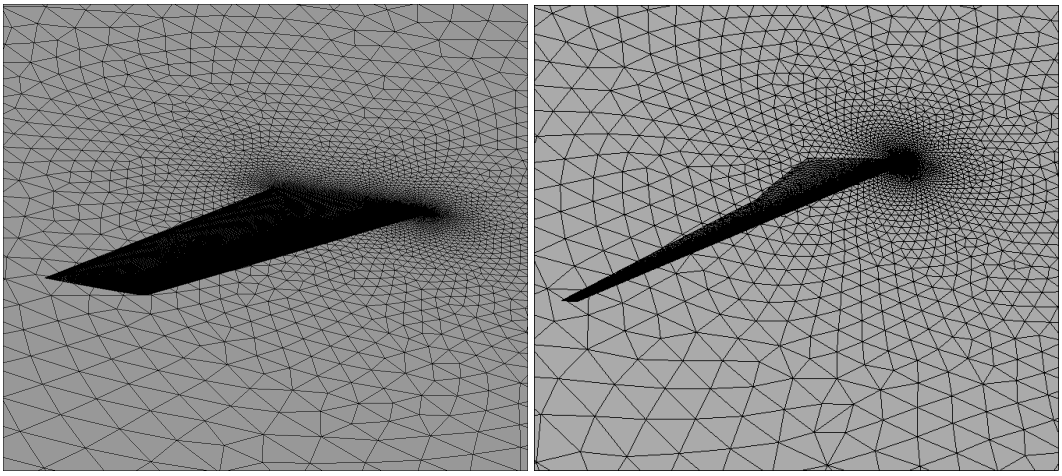

(a) **(b)**

Fig. 3 Aerodynamic surface meshes: (a) AGARD 445.6, and (b) uCRM-13.5

wrapper, or by modifying a small amount of the SU2 source code.

After obtaining a database of GAIC matrices, the p-k method can be used. The p-k method used by Thelen et al. [3] is python based and would be able to be used easily as its own module once the AIC database is generated. A metamodel for the AIC terms can also be employed at this stage. It is a topic for future work to use the doublet lattice method (DLM) as a low fidelity model and the CFD-based simulations as a high fidelity model. These two fidelity levels could be used within a multifidelity cokriging framework similar to Thelen et al. [3].

III. Results

In order to demonstrate the application of this implementation, preliminary results are presented here for the AGARD 445.6 wing and a version of the uCRM-13.5 wing. The results demonstrate the structural and aerodynamic analysis portions of the framework as shown in Fig. 1. While these results represent an intermediate stage of the framework, the cases here were chosen so that they can be compared against current literature and be used as test cases when the rest of the framework has been implemented.

A. AGARD 445.6 wing

The AGARD 445.6 weakened wing is a simple swept wing geometry that will be the first test case. The AGARD 445.6 wing was the subject of 1965 wind tunnel experiments which took place in NASA Langley's transonic dynamics tunnel (TDT) [18]. There are multiple reasons the implementation of this flutter framework is demonstrated on the AGARD wing. First, Thelen et al. [19] studied the flutter behavior of the AGARD 455.6 wing with proprietary analysis software which allows direct comparisons to be made with the results obtained here. Second, the AGARD has been established as a common aeroelastic analysis benchmark case. The planform of the AGARD is shown in Fig. 4. It is a highly swept wing and the airfoil cross-section was chosen as a NACA series airfoil with a thickness of 4% to be consistent with [19]. In experiments, the AGARD 445.6 wing acted as a cantilevered wing, so the spanwise dimension of interest is the semi-span, $b_{\text{semi-span}}$, which is equal to 2.5 ft.

As outlined above, the ESP/CAPS framework was used to model and analyze the AGARD wing. ESP was used to create the model: the design parameters for the planform design of the wing were specified as shown in Fig. 4 and the NACA 0004 airfoil was used for the wing. The structure is modeled with shell elements located on the outer shell of the wing. This structural modeling decision was made to be consistent with Thelen et al. [19].

Following the definition of the model in ESP, the CAPS analysis framework is used to perform the modal analysis and prepare the CFD simulations. The material values for the resulting shell structure are set to the same values as those found by Thelen et al. [19]. The shell structure has a membrane thickness of 16.5 mm, Young's modulus of 5.34×10^8 Pa, shear modulus of 8.31×10^7 Pa, density of 147 kg/m^3, and Poisson's ratio of 0.31. After specifying the material parameters, pyCAPS was used to execute MYSTRAN which extracted the first four modes from the structure.

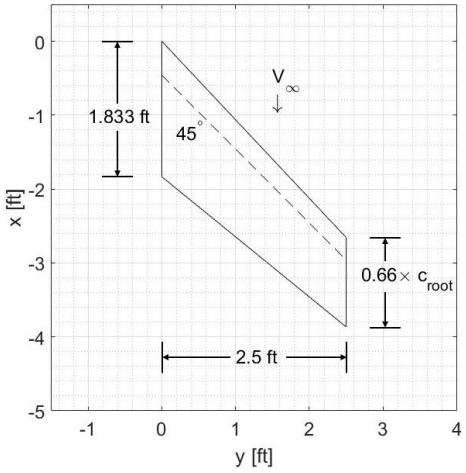

Fig. 4 Planform of the AGARD 445.6 wing

Table 1 Mode frequencies for the AGARD 445.6 wing

Mode	Analysis Frequency (Hz)	Frequencies from [19] (Hz)	Experimental Frequency (Hz)
Mode 1	8.961	9.72	9.60
Mode 2	36.7365	37.34	38.17
Mode 3	46.296	48.85	48.35
Mode 4	90.0421	91.87	91.54

Table 1 summarizes the frequency results for each mode. The modal frequencies from MYSTRAN are listed in the Analysis Frequency column and are 8.961 Hz, 36.7365 Hz, 46.296 Hz, and 90.0421 Hz, respectively. Comparing these frequencies to the experimental frequencies [18] and frequencies from [19] show fairly good correlation, but that MYSTRAN values are consistently low. Before a flutter analysis, the structural model would need to be tuned in order to better match the experimental modal frequencies in a similar way to the inverse design process that was used by Thelen et al. Fortunately, the correlation demonstrates that the structural analysis is set up correctly.

After the modal analysis, a grid convergence study was done to select a mesh for the harmonic CFD simulations. The grid convergence study was done at a Mach number of 0.8 with temperature, pressure, and density values corresponding to the standard atmosphere at sea-level. The mesh sizing parameters were varied while the resulting steady state C_L and C_D values were monitored. Plots of C_L and C_D as a function of the number of volume elements are shown in Fig. 5. C_L levels out near zero since this is a symmetric airfoil, while refining the mesh consistently reduces the value of C_D. In CFD, it is difficult to accurately predict drag. Furthermore, we are neglecting viscous effects with the Euler simulations, so a final mesh was selected based simply on how much C_L changed. Since C_L does not change significantly for a mesh size of 250K, 500K and 1 million volume elements, the harmonic simulations were performed with the 500K mesh.

After the CFD mesh was chosen, CAPS was used to map the mode shapes to the CFD surface mesh of the wing. The first four modes of the AGARD wing mapped to the CFD surface nodes of the AGARD 445.6 wing are plotted in Fig. 5. The color contour represents the z-displacement associated with each mode. These shapes agree with the mode shapes provided on the FUN3D website (cf. [20]).

After mapping the structural mode shapes to the CFD surface mesh, harmonic simulations of each mode are run with SU2 [7]. A flight condition was chosen based upon the experimental flutter conditions at NASA Langley's TDT [18]. The condition selected was run at a density $\rho = 0.0634$ kg/m^3, freestream velocity $V = 307.36$ m/s, and freestream Mach number $M = 0.954$. A reduced frequency of $k = \omega b/V = 0.065$ where b is half of the root chord. This reduced frequency value was chosen because it corresponds to a data point from wind tunnel experiments [18] and because it was studied by Thelen et al. [19]. After specifying the simulation condition, a scaling function (Fig. 7) is applied to the mode shapes to generate the mesh motion files for the harmonic simulations. The scaling function has two

complete cycles that are subdivided into 20 steps each. The amplitude of the scaling function is set so that the maximum displacement is 1% of the root chord length.

The forced harmonic simulations ultimately yield the information that is needed to find the generalized aerodynamic

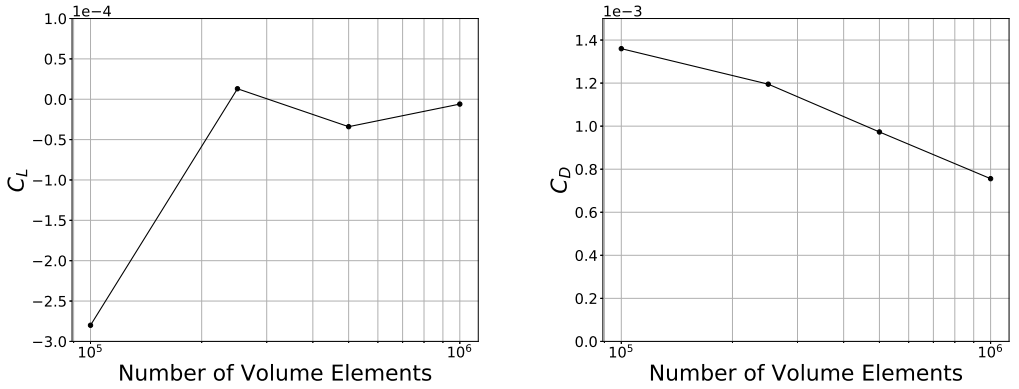

(a) **(b)**

Fig. 5 Mesh convergence study for the AGARD 445.6 wing showing the variation in: (a) the lift coefficient, and (b) the drag coefficient

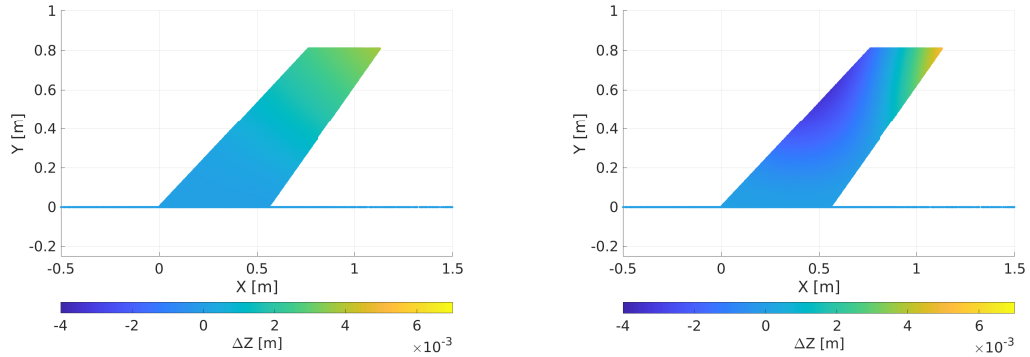

(a) Mode 1 **(b) Mode 2**

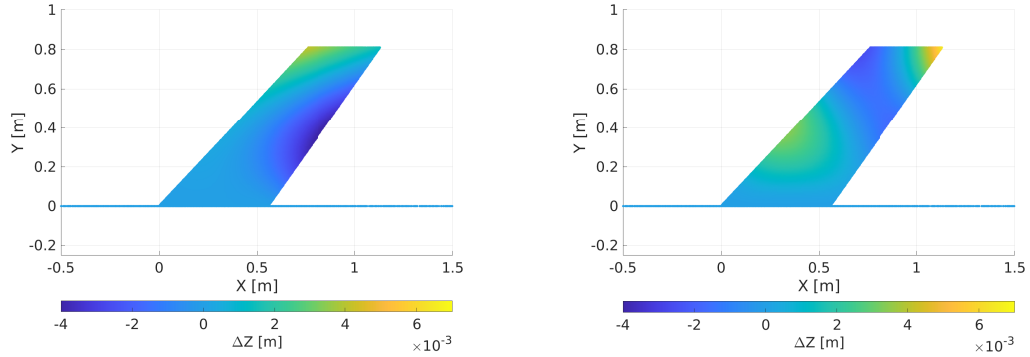

(c) Mode 3 **(d) Mode 4**

Fig. 6 Predicted mode shapes for the AGARD 445.6 wing

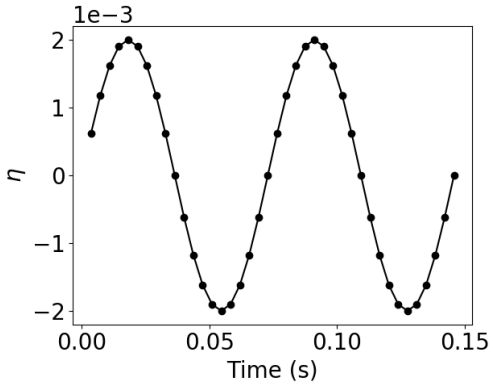

Fig. 7 Modal scaling function for the AGARD 445.6 wing

influence coefficients. Finding the GAIC matrix however requires some post processing and relies on knowing the surface normal vector for each element. Since the implementation of this stage has not been completed yet, variations in the coefficient of pressure will be presented. The steady-state coefficient of pressure halfway between the wing root and wing tip is shown in Fig. 8. The normalized difference between the steady state C_p and the C_p at three different time steps can be seen in Figs. 9a-9d. The time steps that are plotted correspond to the maximum, middle, and minimum points of the scaling function while the wing is in its second cycle of motion. The C_p variations have been normalized with respect to the maximum amplitude of the scaling function (Fig. 7). Therefore, changes in C_p were divided by a factor of 0.002.

The C_p curve at the time step 30 (zero displacement of the mode shapes) is closest to steady state. On the other hand, the C_p curves from time steps 25 and 35 (maximum and minimum displacements) are almost identical. Since the AGARD 445.6 wing uses a symmetric airfoil, this makes sense. Note however that the maximum pressure seen on the wing often lags behind the motion – although time steps 25 and 35 correspond to the the largest value of deflection, the maximum pressure most likely has not been realized yet. This is important to keep in mind when looking at the C_p values in time.

Figure 9 is able to show how C_p is affected by the displacement of the wing in each of its modes. The main focus of future work will be to extract the surface normal information so that the generalized aerodynamic forces can be found for each mode. The calculation of the generalized aerodynamic coefficients would follow directly from this.

B. uCRM-13.5 wing

The first part of the flutter prediction framework is now applied to the undeflected geometry of the uCRM-13.5. The uCRM-13.5 wing analyzed in this work was used by Beren et al. [8] as a model to help study multifidelity modeling applied to an air vehicle. The model is based on the high-aspect ratio uCRM wing published by the University of Michigan MDO Lab [10]. The uCRM-13.5 wing was one of two aerostructural models developed by Brooks et al. [10].

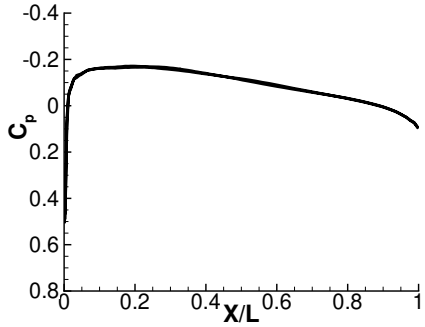

Fig. 8 Steady state C_p for the AGARD wing at y/$b_{\text{semi-span}}$ = 0.5

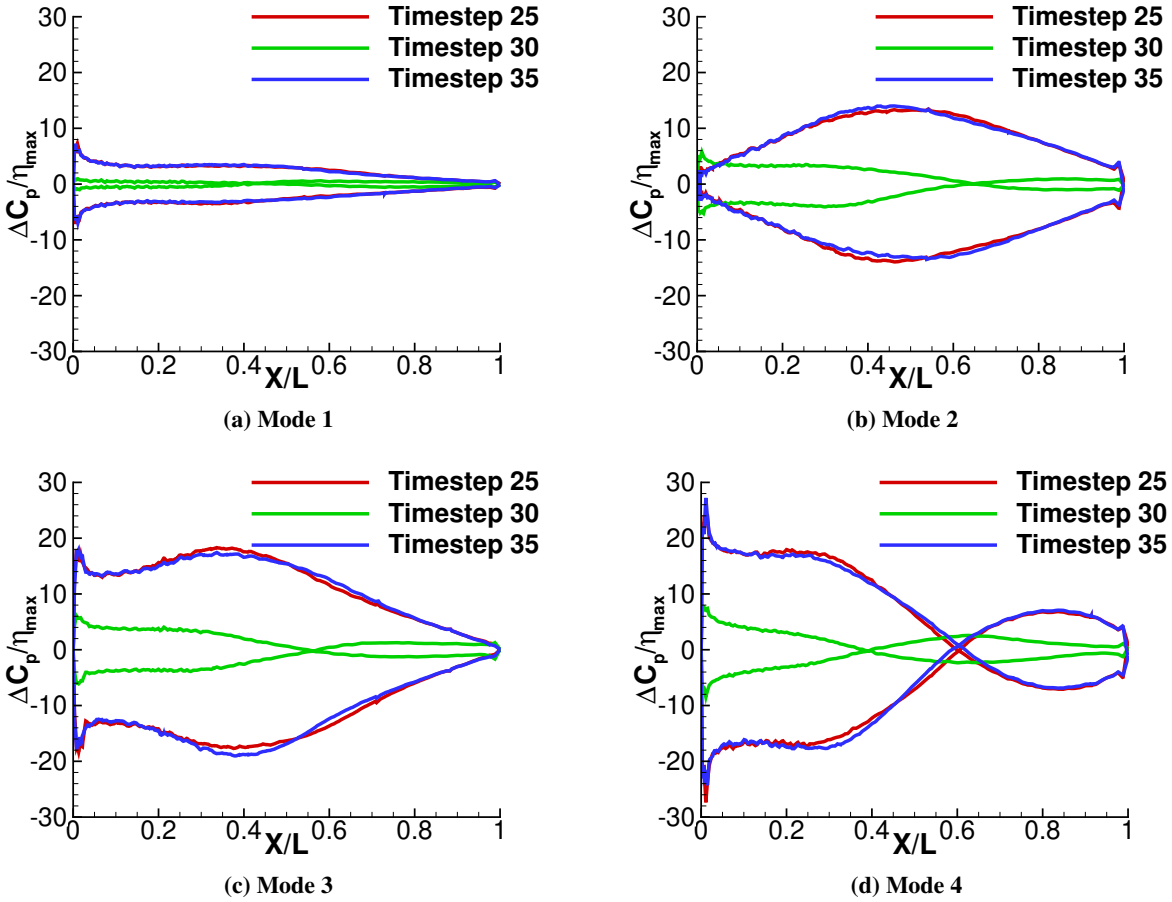

Fig. 9 Time-dependent C_p for the AGARD 445.6 wing at y/b$_{\text{semi-span}}$ = 0.5

The uCRM-13.5 is a high-aspect ratio version of the NASA common research model (CRM) [21]. The University of Michigan MDO Lab developed the uCRM-9 wing which was defined to be "a model with a jig shape and structure that deforms into the shape of the original OML of the CRM model at a nominal cruise condition" [10]. Extending this idea, "the uCRM-13.5 model is the result of a full aerostructural design optimization where the wing OML and the structural sizing are optimized simultaneously" [10].

The undeflected uCRM-13.5 model is parametrized in terms of variables that include the planform area, aspect ratio, outboard wing taper ratio, leading edge sweep, inboard trailing edge sweep, and buttline of the Yehudi break. A plot of the uCRM-13.5 planform used in this paper is plotted in Fig. 10. We will study only the uCRM-13.5 wing as it is plotted in Fig. 10, so the span-wise dimension of interest is $b_{\text{semi-span}}$ which is 35.996 meters. The structure is modeled with a wingbox and by specifying the carry through. The wingbox is modeled with two spars with five ribs in the half-span carry through and 52 ribs in the half-span wing outboard of the wing-fuselage junction. These 52 spars are perpendicular to the leading edge spar.

The structural material is assumed to be aluminum with Young's modulus of 69×10^9 Pa, Poisson's ratio of 0.3, and density of 2,700 kg/m^3. In addition, the element thicknesses for the skin, rib, and spar are shown in Table 2. Finally, there are two structural constraints placed on the wing: the wing is clamped at the centerline and pinned at the wing-fuselage junction.

After building the wing model, MYSTRAN is used to extract the first four modes from the structure. Four modes were chosen to demonstrate the implementation while saving execution time and computational cost. Beren et al. demonstrated the flutter prediction framework on the uCRM-13.5 model by using proprietary analysis codes and give the damping and frequency of the first 10 modes as a function of freestream velocity. These V-f plots from [8] were used as a check to verify our own structural analysis – the mode frequencies when velocity equals zero are shown in

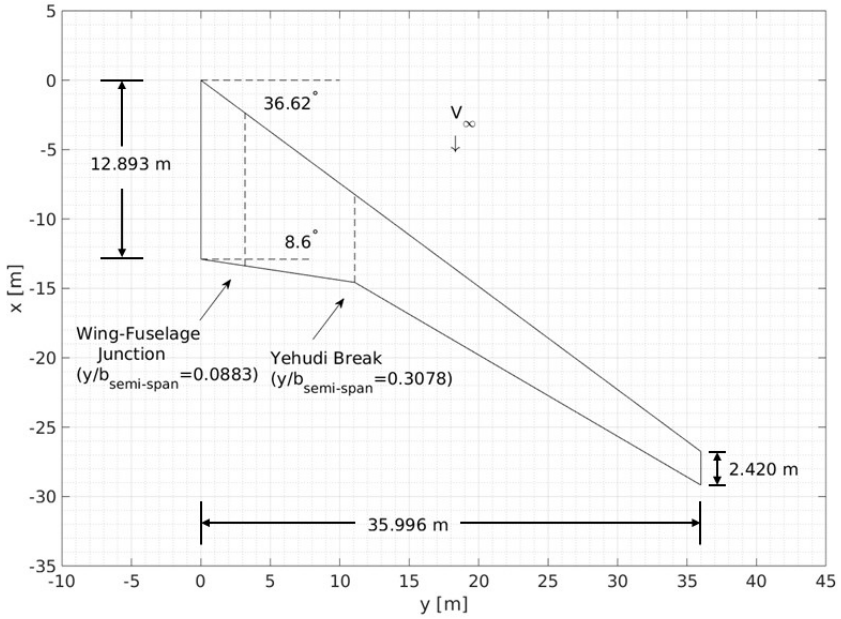

Fig. 10 Planform of the uCRM-13.5 wing

Table 2 Default shell properties for the uCRM-13.5 wing

Structure Type	Membrane Thickness (m)
Skin	0.00254
Rib	10×0.00254
Spar	20×0.00254

column three of Table 3 (note that these values are approximated to the nearest 0.3125 Hz). The frequencies show good correlation with the largest error being 6% for mode 2. Since the work done by Beren et al. focused on multifidelity modeling applied to vehicle optimization, the model parameters of reference [8] may have differed slightly from the parameters used in this work. However, the results correlate closely enough for the current goals of the research.

In preparation for the harmonic CFD simulations, a grid convergence study was done for the uCRM-13.5 wing. The Mach number was set to be 0.8 and the temperature, pressure, and density were equal to their standard atmosphere sea-level values. The aerodynamic mesh was refined as the steady state values of C_L and C_D were monitored. The results from meshes with 100K, 500K, 2 million, and 7 million volume elements are shown in Fig. 11. The C_L value for 2 million elements has a relative error of less than 1% with the C_L value obtained for the 7 million element case and the C_D for 2 million elements has a relative error of about 12% compared to the value obtained with 7 million elements. Similar to the AGARD 445.6 case, C_D varies more than C_L so C_L was the main value that determined which CFD grid

Table 3 Mode frequencies for the uCRM-13.5 wing

Mode	Frequency (Hz)	Frequency when $V_\infty = 0$ (Hz)
Mode 1	0.505049	0.5
Mode 2	1.6698	1.5625
Mode 3	2.77299	2.8125
Mode 4	3.84297	3.75

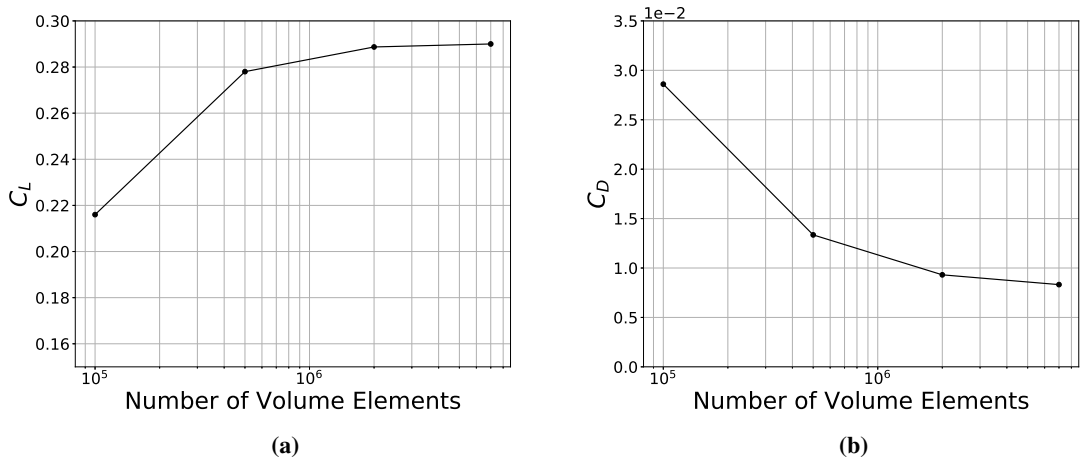

(a) **(b)**

Fig. 11 Mesh convergence study for the uCRM-13.5 wing showing the variation in: (a) the lift coefficient, and (b) the drag coefficient

would be used. Therefore, the harmonic simulations were performed on a grid with 2 million nodes.

After determining the refinement of the CFD mesh, the first four modes of the uCRM-13.5 wing are mapped to the CFD surface nodes. Figure 12 shows the first 4 modes mapped to the CFD surface nodes where the color contour represents the z displacement corresponding to each mode.

Prior to running the harmonic simulations, the mesh motion files need to be written for SU2. Just like the AGARD case, the motion files were written with the help of a script that would read the FUN3D mode shapes and write out the corresponding displacements for each time step. A scaling function was used to ensure that the maximum displacement of the wing would be on the order of 1% of the root chord. The scaling function that was used for the uCRM-13.5 wing is shown in Fig. 13.

For the uCRM-13.5 harmonic simulations, the cruise Mach number was chosen to be 0.85 and the cruise altitude was 37,000 ft. These cruise conditions correspond to the values used in developing the uCRM-13.5 by Brooks et al. [10]. The reduced frequency was chosen to be $k = \omega b/V = 0.1$, where $b = c_{\text{root}}$. This value was chosen based on the fact that reduced frequencies are usually between 0 and 1. When performing the p-k method for multiple values of k, the results from $k = 0.1$ can easily be compared against results at other reduced frequency values.

In the same fashion as the AGARD, the harmonic simulations provide the final step before computing the generalized aerodynamic forces. If the surface normal vectors are extracted, they can be used with the surface pressure values to compute the GAF's. Instead, some results of the pressure coefficient C_p are shown for the uCRM-13.5. These results are measured at two spanwise slices: $y/b_{\text{semi-span}} = 0.35$ and $y/b_{\text{semi-span}} = 0.89$. These spanwise locations were chosen because they are a subset of the spanwise slices extracted by Brooks et al. [10] in the development of the uCRM-13.5 wing.

The results for the steady state C_p on the undeflected uCRM-13.5 geometry are shown in Fig. 14. C_p results are shown for the two separate stations on the uCRM-13.5 wing. Figures 14a and 14b show the C_p results on the wing at stations $y/b_{\text{semi-span}} = 0.35$ and $y/b_{\text{semi-span}} = 0.89$, respectively.

Figures 15 and 16 show how C_p changes on the uCRM-13.5 wing for the harmonic simulations. The spanwise location at $y/b_{\text{semi-span}} = 0.35$ is shown in Fig. 15 while the location at $y/b_{\text{semi-span}} = 0.89$ is shown in Fig. 16. At each station, four plots are shown which correspond to mode 1, mode 2, mode 3, and mode 4 respectively. Within each plot, three curves are drawn, corresponding to 3 time steps from the harmonic simulations. As in the AGARD case, each curve shows the normalized difference between C_p and the steady state C_p value. The difference has been normalized by the maximum amplitude of the scaling function. This normalized difference allows us to see how deflection in each mode affects C_p. Similar to the AGARD 445.6 results that are in Fig. 9, we can see that C_p at time step 30 matches closely with steady state. For time steps 25 and 35, the two plots are almost mirror images of one another, however some modes show that the time steps 25 and 35 are not exact mirror images of one another. This could possibly be because the uCRM-13.5 does not have a symmetrical airfoil like the AGARD 445.6 wing does. Despite the fact that the pressure is not an exact mirror image between time steps 25 and 35, if we look at the magnitude values they are nearly

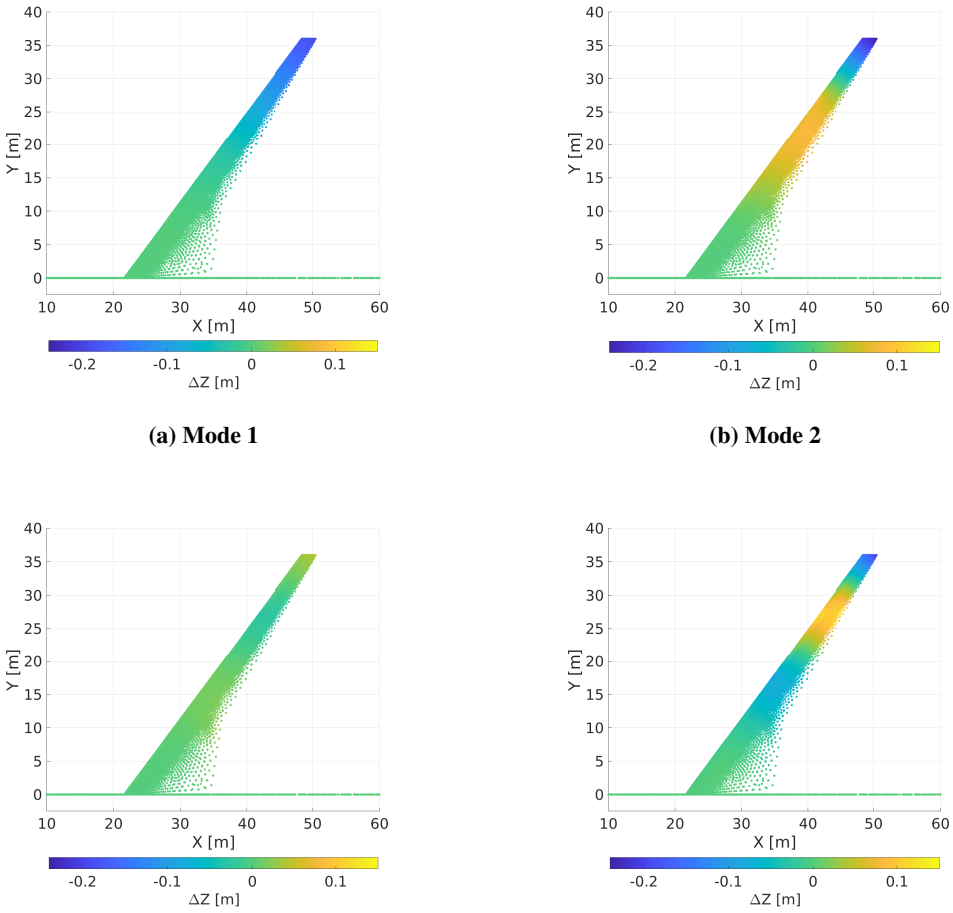

(a) Mode 1 **(b) Mode 2**

(c) Mode 3 **(d) Mode 4**

Fig. 12 Predicted mode shapes for the uCRM-13.5 wing

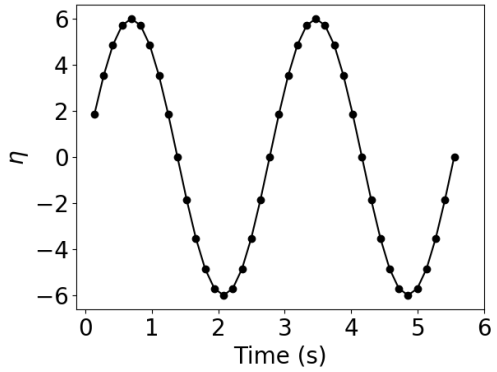

Fig. 13 Mode scaling function for the uCRM-13.5 wing

equal. This agrees with the idea that for small displacements, pressure should be a linear function of displacement.

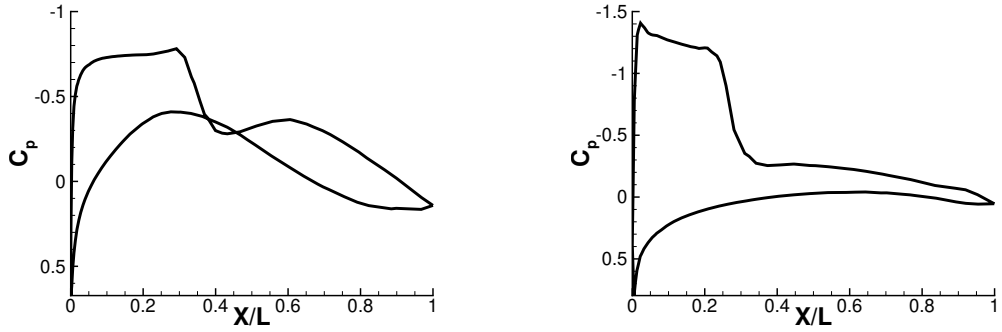

(a) $y/b_{semi\text{-}span} = 0.35$ (b) $y/b_{semi\text{-}span} = 0.89$

Fig. 14 Steady state C_p for the uCRM-13.5 wing

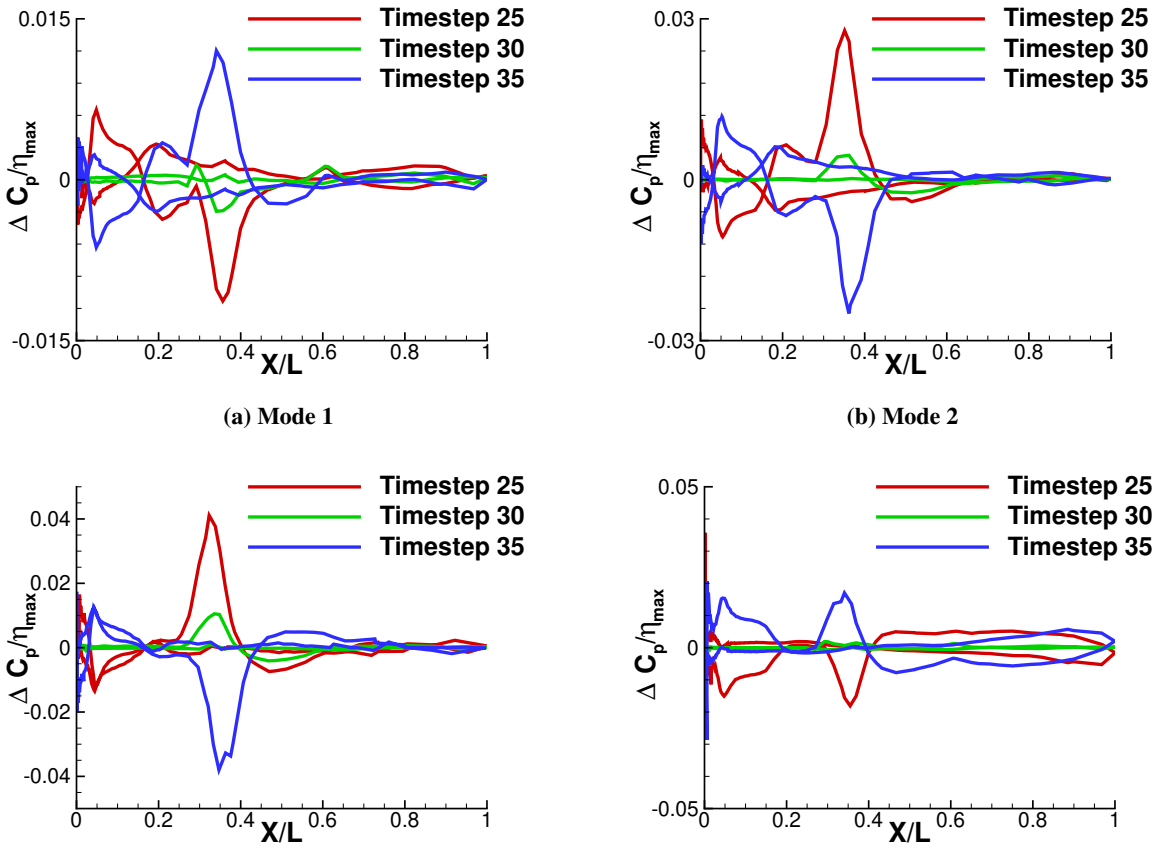

(a) Mode 1 (b) Mode 2

(c) Mode 3 (d) Mode 4

Fig. 15 Time-dependent C_p for the uCRM-13.5 wing at $y/b_{semi\text{-}span} = 0.35$

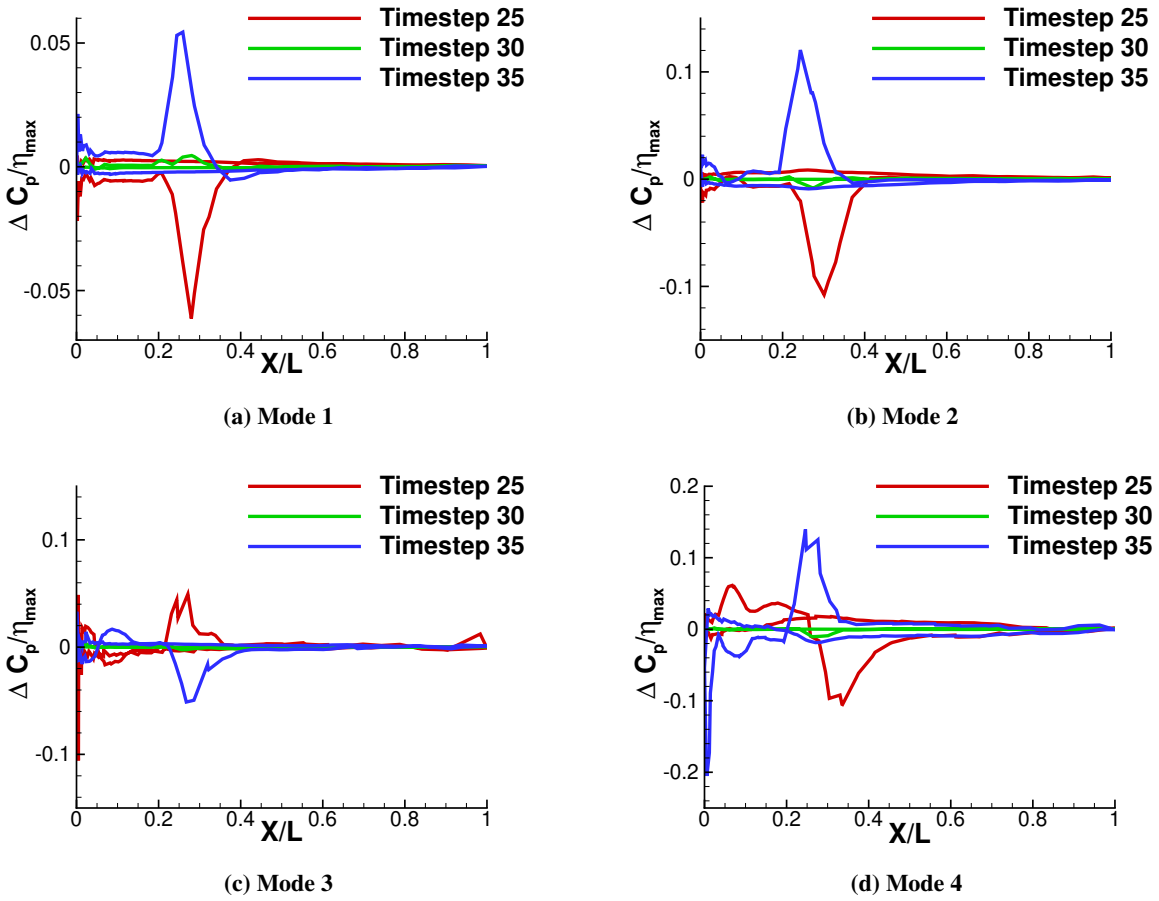

(a) Mode 1

(b) Mode 2

(c) Mode 3

(d) Mode 4

Fig. 16 Time-dependent C_p for the uCRM-13.5 wing at $y/b_{\text{semi-span}} = 0.89$

IV. Conclusion

The first half of a flutter analysis workflow has been used to perform harmonic CFD simulations on the AGARD 445.6 wing and the uCRM-13.5 wing. These wings were of particular interest because the AGARD has been used extensively as an aeroelastic benchmark case while the uCRM-13.5 represents the geometry of a contemporary, high-aspect ratio transport aircraft. The CFD results on these two wings were obtained with open-source software and the results were briefly compared to previous literature to demonstrate the successful implementation of the code. Furthermore, since open-source software was used for the structural and CFD analyses, the analysis codes that were used for this work are freely available for the online community to explore and use. The implementation was described along with current challenges that are being faced. The purpose of this paper is to describe the implementation of the first half of a flutter prediction framework and provide a review of the future work needed to complete the framework.

While this paper represents only the first half of the flutter prediction process, finishing the framework will be the focus of future work. The key steps left are to compute the CFD-based GAIC matrices and then to set up the metamodeling and p-k method around the analysis process. Computing the CFD-based GAIC matrices was originally done in FUN3D by using surface normal information on the wing. SU2 does not publicly display this information, and part of future work will focus on obtaining this information. The authors suspect that it may be possible to use surface normal data by using the Python Wrapper for SU2. Another potential solution may be to modify the SU2 source code responsible for computing and printing CFD information. The metamodeling and p-k method that the present authors intend to use were written by Andrew Thelen as part of his PhD Research. As these codes are already available, future work will focus on the data flow from the CFD analyses to the iterative p-k method. The metamodel and p-k method together will allow the user to determine flutter data which will include the ability to create plots of flutter speed vs. Mach number or flutter frequency vs. Mach number.

Acknowledgements

This project/material is based upon work supported by the Iowa Space Grant Consortium under NASA Award No. NNX16AL88H. The second and third authors are supported by NSF award number 1846862.

References

[1] Opgenoord, M. M. J., Drela, M., and Willcox, K. E., "Influence of transonic flutter on the conceptual design of next-generation transport aircraft," *AIAA Journal*, Vol. 57, No. 5, 2019, pp. 1973–1987.

[2] Jonsson, E., Riso, C., Lupp, C. A., Cesnik, C. E., Martins, J. R., and Epureanu, B. I., "Flutter and post-flutter constraints in aircraft design optimization," *Progress in Aerospace Sciences*, Vol. 109, 2019, p. 100537. doi:https://doi.org/10.1016/j.paerosci.2019.04.001.

[3] Thelen, A., Leifsson, L., and Beran, P., "Aeroelastic flutter prediction using multi-fidelity modeling of the aerodynamic influence coefficients," *AIAA SciTech Forum*, San Diego, CA, January 7-11, 2019.

[4] MSC Software Corporation, "MSC Nastran - Multidisciplinary Structural Analysis," 2020. URL https://www.mscsoftware.com/product/msc-nastran.

[5] Biedron, R., Carlson, J.-R., Derlaga, J., Gnoffo, P., Hammond, D., Jones, W., Kleb, B., Lee-Rausch, E., Nielsen, E., Park, M., Rumsey, C., Thomas, J., and Wood, W., *FUN3D Manual: 13.2*, 2017. URL https://fun3d.larc.nasa.gov/papers/FUN3D_Manual-13.2.pdf.

[6] Case, B., "MYSTRAN - General Purpose Finite Element Structural Analysis Computer Program," 2020. URL https://www.mystran.com/.

[7] Economon, T. D., Palacios, F., Copeland, S. R., Lukaczyk, T. W., and Alonso, J. J., "SU2: An open-source suite for multiphysics simulation and design," *AIAA Journal*, Vol. 54, No. 3, 2015, pp. 828–846.

[8] Beran, P. S., Bryson, D., Thelen, A. S., Diez, M., and Serani, A., "Comparison of Multi-Fidelity Approaches for Military Vehicle Design," *AIAA AVIATION Forum*, Virtual Event, June 15-19, 2020. doi:10.2514/6.2020-3158, URL https://arc.aiaa.org/doi/abs/10.2514/6.2020-3158.

[9] Laboratory, M. D. O., "uCRM: undeflected Common Research Model," 2020. URL https://mdolab.engin.umich.edu/wiki/ucrm.html.

[10] Brooks, T. R., Kenway, G. K. W., and Martins, J. R. R. A., "Benchmark Aerostructural Models for the Study of Transonic Aircraft Wings," *AIAA Journal*, Vol. 56, No. 7, 2018, pp. 2840–2855. doi:10.2514/1.J056603, URL https://doi.org/10.2514/1.J056603.

[11] Johnson, E., and Venkayya, V., *Automated Structural Optimization System (ASTROS)*, Vol. I - Theoretical Manual, 1988.

[12] Rodden, W., Harder, R., and Bellinger, E., "Aeroelastic Addition to NASTRAN," *NASA Contractor Report 3094*, 1979.

[13] Forrester, J. I. A., Sobester, A., and Keane, J. A., *Engineering Design via Surrogate Modelling: A Practical Guide*, John Wiley and Sons, Ltd., New York, 2008, pp. 33–76. doi:10.1002/9780470770801.

[14] Haimes, R., and Dannenhoffer, J., "The Engineering Sketch Pad: A solid-modeling, feature-based, web-enabled system for building parametric geometry," *21st AIAA Computational Fluid Dynamics Conference*, San Diego, CA, June 24-27, 2013.

[15] Durscher, R., and Reedy, D., "pyCAPS: a Python interface to the Computational Aircraft Prototype Syntheses," *AIAA SciTech Forum*, San Diego, CA, January 7-11, 2019.

[16] Haimes, R., and Drela, M., "On The Construction of Aircraft Conceptual Geometry for High-Fidelity Analysis and Design," *50th AIAA Aerospace Sciences Meeting including the New Horizons Forum and Aerospace Exposition*, Nashville, TN, January 9-12, 2012. doi:10.2514/6.2012-683.

[17] Marcum, D. L., and Weatherill, N. P., "Unstructured grid generation using iterative point insertion and local reconnection," *AIAA Journal*, Vol. 33, No. 4, 1995, pp. 1619–1625.

[18] Yates Jr., E. C., "Standard Aeroelastic Configurations for Dynamic Response I - Wing 445.6." *AGARD Report No. 765*, 1988.

[19] Thelen, A., Leifsson, L., and Beran, P., "Multifidelity flutter prediction using local corrections to the generalized AIC (IFASD-2019-062)," *International Forum on Aeroelasticity and Structural Dynamics (IFASD)*, Savannah, GA, June 10-13, 2019.

[20] Silva, W. A., Perry III, B., and Chwalowski, P., "Evaluation of Linear, Inviscid, Viscous, and Reduced-Order Modeling Aeroelastic Solutions of the AGARD 445.6 Wing using Root Locus Analysis," *AIAA SciTech*, National Harbor, MD, January 13-17, 2014.

[21] Vassberg, J., Dehaan, M., Rivers, M., and Wahls, R., "Development of a Common Research Model for applied CFD validation studies," *26th AIAA Applied Aerodynamics Conference*, Honolulu, HI, August 18-21, 2008.